Shape-Controlled Growth of Metal Nanoparticles: An Atomistic View [a]

Mine Konuk

Department of Physics, Istanbul Technical University, Maslak 34469 Istanbul, Turkey

Faculty of Science and Letters, Piri Reis University, Tuzla 34940 Istanbul, Turkey

Sondan Durukanoğlu

Faculty of Engineering and Natural Sciences,

Sabancı University, Tuzla 34950 Istanbul, Turkey

Nanotechnology Research and Application Center,

Sabancı University, Tuzla 34950 Istanbul, Turkey

(Dated: November 4, 2015)

Recent developments in shape-controlled synthesis of metallic nano-particles present a promising path for precisely tuning chemical activity, selectivity, and stability of nano-materials. While previous studies have highlighted the macroscopic description of synthesis processes, there is less understanding as to whether individual atomic-scale processes posses any significant role in controlling growth of nano-products. The presented molecular static and dynamic simulations are the first simulations to understand the underlying atomistic mechanisms of the experimentally determined growth modes of metal nano-clusters. Our simulations on Ag nano-cubes confirm that metal nano-seeds enclosed by {100} facets can be directed to grow into octopod, concave, truncated cube, and cuboctahedron when the relative surface diffusion and deposition rates are finely tuned. Here we further showed that atomic level processes play a significant role in controllably fine tuning the two competing rates: surface diffusion and deposition. We also found that regardless of temperature and initial shape of the nano-seeds, the exchange of the deposited atom with an edge atom of the seed is by far the governing diffusion mechanism between the neighboring facets, and thus is the leading atomistic process determining the conditions for fine tuning of macroscopic processes.

[a] Electronic supplementary information available

I. INTRODUCTION

In recent years, metallic nano-structures have attracted considerable attention as they exhibit exceptional size/shape dependent properties and greatly enhanced performances in many industrially and technologically important phenomena such as catalysis, chemical reactivity, selectivity, and stability [1–6]. Evidently, to utilize such minuscule particles with specific morphology and architecture requires precise control of the growth and structure. Thanks to the outstanding works of several groups, tuning of growth conditions, with a sufficient degree, to decipher the rules governing the evolution of the growth front [7–13], and thus to tailor nano-crystals with certain structural, chemical, optical, and magnetic characteristics is now possible [14, 15]. In general, formation of nano-crystals in a synthesis is history-dependent and driven by two intimately and intricately linked processes: thermodynamic and kinetic. In a thermodynamically controlled process the morphology of final product is governed by the minimization of the total energy whereas in a kinetically guided process the product is shaped through the manipulation of reaction conditions [7, 8]. Although the key questions concerning the ability to further fine-tune a thermodynamic/kinetic process and to improve the yield of nano-structures with precise architecture are clearly related to the growth details at the atomic scale, specially at the earliest stages of growth mode where a metal seed transform into a nano-particle with a different shape, much of the focus in controlling the morphology of final product has been on the overall macroscopic description of synthesis process and it still remains a great challenge to atomically monitor the formation of nano-particles under varying growth conditions.

Nano-materials are usually enclosed by combinations of low index surfaces and adatom diffusion on these surfaces is by far the most important kinetic process in shaping the morphology of the material [16, 17]. Smooth facets on these materials could not be formed unless atoms have sufficient mobility at surfaces. From the studies of solution phase synthesis of metal nano-crystals, it is known that surface diffusion of atoms at the facets of a growing seed plays a critical role in determining the growth front of the seed and thus controlling the final shape and morphology of the end-products [18, 19]. In an excellent experimental work on Pd nanocubes, it was further shown that morphology of a growing nano seed is determined by the interplay between the rates of deposition and surface diffusion[20]. However, identifying atomistic details involved in a typical crystal growth process is not easy, in

particular when the crystal growth occurs in solution[21]. To this end, atomistic simulations are real alternative to examine the structure and dynamics of growing particles at the atomic scale and thereby specify the important individual atomistic processes taking place in the course. Herein, using extensive molecular static and molecular dynamic calculations we reproduced the growth modes, proposed in Ref. [20], on silver nano-particles and examined the individual atomic processes and regarding energetics that influence the morphological evolution of growing particles. Therefore, this work not only confirms and explains recent shape-controlled synthesis results[20], but also provides a quantitative atomic view of how exactly surface diffusion of atoms could control the shape evolution of nano-particles for better design.

The rest of this report is organized as follows. While geometries of the investigated clusters and diffusion mechanisms, together with computational techniques are briefed in Sec. II, the adsorption energies and energy barriers for specific diffusion events are presented in Sec. III. Results of MD simulations are discussed in Sec. IV and our concluding remarks are summarized in Sec. V.

II. GEOMETRIES AND COMPUTATIONAL DETAILS

The model systems for examining the growth of cubic Ag nano-clusters are carefully chosen to simulate more realistic representations of experimentally investigated metal nano-structures[20]. All computational cells are bounded by six {100} facets, eight {111} facets at the corners and twelve narrow {110} facets at the edges, with each having different number of atoms along the periphery of {111} facets. In this work, we specifically focused on two types of cubic structure: Type I and Type II (see Fig. 1(a) and Fig. 1(b)). Although the length of each cubical system is the same, 3.6 nm, they differ from one another in that Type I cubic cell involves two atomic chains of <110> at the edges whereas Type II contains three chains of <110> atoms. The number of atoms along the periphery of {111} facets on Type I and Type II systems is, respectively, 15 and 12.

Adatoms may hop or exchange at the edges/facets. In a hopping mechanism to cross an edge, the adatom simply jumps over the edge to the next lattice site on the neighboring facet while in an exchange mechanism, it directly kicks the edge atom to the next site on the adjacent facet and takes its place (see Fig. 2). The diffusion processes involved in

this work are shown in Fig. 2. The green spheres represent the mobile atoms involved in various diffusion processes, and the spheres labeled 0, 1, 2, and 3 represent the atoms in the proximity of the adatom along the edges, participating in exchange mechanisms. In the figure, the exchange processes are indicated by X, while the hopping processes are represented by H. The superscripts denote the atoms by which the exchange process is executed. The expression in the subscripts, on the other hand, denotes the diffusion path from/to facets.

In all simulations the atoms in the model systems are initially arranged in their perfect lattice positions and allowed to interact via potentials obtained from the embedded atom method (EAM)[22]. These potentials are based on Quantum Mechanical approximations and have proven to be reliable in accurately describing many characteristics of nano-structured materials [23–28]. The standard conjugate gradient method is utilized to fully minimize the total energy of the system. Molecular static (MS) and dynamic (MD) simulations are carried out after eliminating non-zero initial stress in the model systems. In MD simulations, atoms are coupled to a Nosé-Hoover thermostat [29, 30] to keep systems in the equilibrium at higher temperatures and equations of motion are integrated with steps of 1 fs using the Verlet algorithm. All MD simulations have been performed using the MD code, LAMMPS, developed by Sandia National Laboratory[31]. Activation energy barriers for diffusion processes are calculated using an accurate and efficient technique of the 'Nudged Elastic Band' (NEB)[32, 33]. The method essentially generates the minimum energy path between the initial and final states of the system by generating "a chain of states" of the system for the intermediate states in configurational space and then carrying out a simultaneous optimization procedure for the intermediate states. The saddle point and hence the energy barrier for the process is given by the highest energy along the path.

III. ADSORPTION AND ACTIVATION ENERGIES

Since the goal in this study is to determine the role of atomic processes in the interplay between rates for atom deposition and surface diffusion that governs the growth pathway of a seed[20], we first calculate the energetics associated with a single atom diffusing on a facet on the cubic system. Evidently, in the earliest stages of the growth, deposited atoms have multiple available adsorption sites on/around {111} facets before initiating nucleation and

due to the finite size effects, adsorption sites around these facets posses varying energetic characteristics. We, therefore, calculated relative adsorption energies for several sites with respect to the center of the {111} facet (for the sites, see Fig. 1(c) and Fig. 1(d)) and tabulated the results in Table 1. All the adsorption sites close to the edges are energetically more favorable than the center site, A. On Type I cubic system, the site C on {110} facet has the deepest potential well, followed by the sites H, K on {100} facet, and B on {111} facet. Thus Ag adatoms deposited on the corner facet would energetically favor the sites at the edges rather than the center.

When deposition is confined to only {111} facets, then the growth on the narrow {110} and large {100} facets are largely controlled by how often the adatoms deposited on the {111} facets cross the edges where the facets meet. Clearly, of the key factors determining the attempt frequencies of all relevant diffusion processes and thus the evolution of the surface morphology is the activation barrier that adatoms ought to overcome. The energy barrier involved in the process strongly depends on the local atomic geometry. Here, we specifically focused on the elementary diffusion processes between different facets that are primarily relevant to the shape evolution of a growing crystal (see Fig. 2) and presented the regarding energy barriers in Table 2. In addition, the potential energy profiles for a few selected diffusion processes are plotted in Fig. 3. The snapshots of the process at specific adsorption sites are shown in the insets. Note that energy zero is the energy of the system when the adatom (green sphere) is absorbed on the site A and the relative energies of other sites are given with respect to A. The barrier heights presented in Table 2 are given with respect to the initial adsorption site of the process near the edge on {111} facet (see Fig. 3). As clearly seen in the table, the most favorable diffusion process between the facets is the exchange from {111} to {110} facet via *atom 1* on Type I and via *atom 0* on Type II cubic systems. It should be pointed out that in contrast to the case on Type I cubic system where there is only one channel to diffuse to {110} facet (through *atom 1*), on Type II cubic system, the adatoms find another favorable exchange mechanism through *atom 0* with an activation barrier of 0.15 eV which is 35% less than that of the exchange via *atom 1*. Hopping to {110} and {100} facets are less favorable, with the respective activation barriers of 0.32 eV and 0.34 eV. Diffusions from {111} to {100} facet are interestingly less favorable than those to {110} facet. Total energy calculations on larger cubic seeds (see Fig. S1) did not change the observed energetic characteristics (see Table S1). Thus, from energetic

perspective, regardless of the initial shape of cubic seeds the adatom deposited on {111} facet would preferentially migrate to the edges to find energetically more favorable sites on the {111} facet and then would diffuse to the neighboring {110} facets through an exchange mechanism, in particular.

IV. MD SIMULATIONS

Although the picture portrayed by the energetics provides valuable insights into the mechanisms that may be important in the growth of Ag nano-cubes, it does not give the full description as growth is a non-equilibrium process with a number of effects that are of manifestly kinetic origin such as deposition and diffusion. Surface diffusion, in particular, is a thermally activated process that reflects the strong influence of temperature on the morphology of a growing crystal. We thus performed MD simulations on both types of Ag cubic systems to determine the underlying growth kinetics. We first conducted calculations for the Root Mean Square Displacements of the atoms on cubic clusters similar to the calculations performed on polyhedral clusters[17], second collected the MD data to determine the statistical nature of single atom processes, and finally performed MD simulations to identify atomic nature of growth modes.

A. Root Mean Square Displacements

As the systems under consideration are composed of {111}, {110}, and {100} facets, the mobility of single adatoms on these three different facets is investigated by calculating the root mean square displacements (RMSD) of atoms in different layers. In Fig. 4, we have plotted RMSD's of atoms, as a function of temperature, in varying layers of each facet of Type I system. As shown in the figure, to calculate the RMSD's of different layers for each facet three initial configurations were utilized (see the insets in Fig. 4). For the {111}, {110}, and {100} configurations, one adatom was separately placed closed to the center of eight corner, of twelve edge, and of six side facets, respectively. The average potential energy of the adatoms on the respective facets, as a function of temperature, is also plotted on the right in Fig. 4.

Note that while the adatoms on {110} and {100} facets keep their initial lattice sites up

to temperatures 450 K, those on {111} become mobile around 50 K, above 100 K they are in close vicinity of the edges, and between 300 K and 400 K they already exchange positions with the {111} facet atoms at the borders and some diffuse to the neighboring facets. The fact that the average potential energy of the adatoms on {111} around 400 K decreases to -2.2 eV also suggests that majority of adatoms exchange their position with {111} facet-atoms by which an adatom increases its coordination number and thus the potential energy. Around 500 K some adatoms diffuses to the edge facets of {110} (see the configuration at 600 K in Fig. 4(a)) and this is seen as a convergence to the low-temperature average potential of the adatoms on {110} facet (-2.1 eV, see Fig. 4(b)). The high mobility of adatoms on {111} facets is in compatible with our previous results of adsorption energies and low activation energy barriers for the sites on {111} facets (see Fig. 3). It is also interesting to note that RMSD's of atoms in the second and third layer (blue and green colored atoms) increase noticeably above 650 K which points to initiation of interlayer exchange of atoms. Keep in mind that the second and the third layer atoms are interior atoms and their interchange between the neighboring layers initiate disordering on the system. As clearly seen in Fig. 4(a), disordering of {111} facets is initiated around 750 K.

The RMSD's of adatoms on {110} and {100} facets below 400 K, on the other hand, are essentially due to lattice vibrations and the adatoms more or less keep their initial lattice sites. There is a steady increase in both average value and fluctuations of the potential energy of adatoms, up to 500 K, which is induced by thermal expansion with increasing temperature. From the RMSD of adatoms on {100} facets, it is clearly seen that the adatoms migrate to neighboring lattice sites around 500K and above 600 K they hop larger distances. While the atoms on {110} start exchanging their position with substrate atoms around 550 K, which is seen as a sharp decrease in potential energy, those on {100} facets don't exchange with the substrate atoms before they reach close to the edges which happens around disordering temperature of {110} facets (700 K, see Fig. 4(b)).

B. Statistics on Atomic Processes

To see how the mobility of an adatom on the {111} facets changes with respect to temperature, we run MD simulations of 300 repeated events of a diffusing single atom at varying temperatures, ranging from 300 K to 600 K. Each simulation starts with deposition of the

adatom to the corner facet and ends once the adatom diffuses from the corner to the side/edge facets of {100} and {110}. For 300 repeated events of each temperature, the adatoms are initially configured at a distance of 6 Å above the {111} facet with random thermal velocities corresponding to the specific temperature of the system and next deposited on the corner facets. On the average, the adatoms land on the corners in 15 ps (for landing position distribution see Fig. S2). The motion of the adatom on the {111} facet is then traced from the time it lands on the facet to the time it diffuses to the nearby facets, either {110} or {100}, by one of the specific diffusion mechanisms described in Fig. 2. After observing the border-crossing event, the nature of crossing was recorded: the type of mechanism and the time for the transition to take place (from landing on the corner to diffusing to the neighboring facets). The statistics for a total of 300 repeated events for each temperature are presented in Fig. 5. The MD results confirm the energetic predictions of the previous section: regardless of temperature, the leading diffusion mechanism in the mobility of a single atom from {111} facet to the other facets is by far the exchange of the adatom with an edge atom. Notable number of hopping attempts occurs only when temperature is high enough. At low temperatures (300 K and 350 K) the growth of the Ag cubic seeds, at least in the early stage, is mainly limited to the <110> direction due to higher attempt frequency of the adatom to diffuse to {110} facets relative to {100} facets (Fig. 5(c)). As seen in Fig. 5(a), on Type I Ag cubic system moderate number of diffusion events to {100} facets appears to happen above 350 K, whereas on Type II it is quite difficult up to temperatures close to 550 K.

The average diffusion times for border-crossing events from the corner to either one of the {110} and {100} facets for Type I and II systems are, respectively, presented in Table 3 and 4. The average values are based on the corresponding number of diffusion events, that are also included in the tables. Note that for each of 300 repeated events, the simulation is carried on till the adatom crosses the border and diffuses to either facets ({110} or {100}). A quick glance at these table leads to the following observations: *i*) regardless of temperature, the majority of events results in a diffusion to {110} facets; *ii*) while border-crossing events to {100} side facets at low temperatures are either non-exist or statistically insignificant, these events become noteworthy with increasing temperatures; *iii*) for all border crossing events, average diffusion time decreases with increasing temperature as expected; *v*) once another {110} channel is introduced to the system as in Type II, diffusions to side facets

become statistically insignificant up to 450 K; *vi*) although the average diffusion times for the diffusions to {110} and {100} facets converge to a resembling value with increasing temperatures, majority of the diffusion events happens to the edge facets.

On Type I system the timescale of diffusion events to {110} facets between 300 K ($1/(k_bT) \approx 38$ eV^{-1}) and 500 K ($1/(k_bT) \approx 21$ eV^{-1}) varies by 1.5 times compared to that on Type II system (Fig. 5(c)), owing to the larger activation barriers (see Table 2). As clearly seen in Fig. 5(c), there is a pronounced effect of local morphological differences on the attempt frequency of a single atom diffusion at low temperatures, being several order of magnitude larger for Type I than Type II. However, the effect weakens with increasing temperatures, leading to almost a morphology independent diffusion characteristic. It is also worth to note that on both types of cubic systems the attempt frequencies for diffusions from {111} to {100} facets are substantially low and become statistically significant only after 450 K ($1/(k_bT) \approx 25$ eV^{-1}) (see inset in Fig. 5(c)). Since the attempt frequency at low temperatures is quite low, growth of aggregates on the {111} facets is expected to be confined by adsorption and diffusion to the other facets is less likely. We have also traced the individual diffusion processes for the interlayer mass transport between {111} and {100}, {110} facets. For the adatom on {111} facet of Type I Ag cubic system, the only possible exchange mechanism to {110} facet is via *type 1 atom* (for atom labeling, see Fig. 2), and thus all exchange diffusions occurs through the *type 1 atom*. On the other hand, because the {111} facet has longer length along the {100} facet, exchange diffusion to {100} facet involves several atoms, mostly through *type 2 atom*, followed by *type 1*, and then *type 3*. For the diffusions to {100} facets, the most frequent mechanism is, interestingly, not the one specified by the lowest energy barrier: the adatom can easily cross to a {100} facet through an exchange mechanism which bears larger activation barrier compared to a direct hopping (see Table 2). However, once there is a change in the peripheral morphology of the {111} facet as in Type II cubic system, the interlayer mass transport between {111} and {110} facets is expected to be predominantly governed by the exchange of the adatom with the middle edge atom (*atom type 0*) instead of corner edge atom (*atom type 1*). More interestingly, presence of even one extra chain along the <110> edges almost eradicates diffusions to {100} facets. Even at 500 K, the adatom preferentially diffuses to the {110} facets rather than to {100} with 94% of the 300 events compared to the 66% on Type I cubic system. However, when the length of the two cubic systems was increased from 3.6

nm to 6.1 nm while keeping the main characteristics in morphology of the facets unchanged, albeit in scaling differences, the energetics and statistical characteristics remained similar (Fig. S3).

C. Growth Simulations

In order to determine the atomistic nature of the growth modes, we have simulated growth on various silver nano-seeds. To make the processes faster and simulations computationally and timely affordable, MD runs are carried out at 500 K. The temperature and deposition rates in the simulations are identified on the basis suggested by the statistics of repeated 300 single adatom diffusion events on the cubic Ag clusters. Herein, the growth simulations have been run on Type I Ag cubic system with varying deposition rates. Similar to the previous MD simulations on statistics, the adatoms are initially placed 6 Å away from the corner facets and thermalized at 500 K with the rest of the system. Atoms are then deposited one by one on a randomly chosen {111} facet of the cubic system until a specific type of growth mode is observed. The number of deposited atoms varies from 200 to 700 depending on the growth mode. It takes about 15 ps for the adatoms to land on the corner facets. In short, the MD simulation for growth starts with deposition of adatoms from 6 Å away from the corners of the cubical system and ends once a specific growth mode is observed. To further test the concluding remarks similar growth simulations on Type II cubic system are also conducted.

Our growth simulations on cubic Ag nano clusters confirm the principles set in the experiment on Pd nano-cubes: the interplay between the rates of deposition and surface diffusion determines the growth pathway of the metal nano-seed and under the specific conditions determined in the experiment[20], the observed growth modes have been successfully reproduced. In Fig. 6, we present snapshots of the observed growth modes: (a) After deposition of 500 atoms with a rate of one atom each 30 ps, an octopod shaped structure is obtained. At this relatively fast deposition rate with respects to 250 ps of the average time to cross the edge (see Table 3), the adatoms simply do not have enough time to diffuse to the other facets before building aggregates on the {111} facets, thereby lead to 3-D and localized growth where they land, with the branches extending in <111> direction. Let us mind that in the simulations atoms were deposited one by one on one of the corner facets and it would take at

most 240 ps (8 corner facets×30 ps) for the next atom to land on the same facet which is still not sufficient for the deposited atoms to diffuse to other facets before initiating nucleation on the facets they are adsorbed. (b) At deposition rate of one atom each 100 ps the adatoms can form small aggregates on {111} facets but a small number of atoms diffuses to the edges and side facets of the cube, and thus resulting in a concave structure after deposition of 500 atoms. Again, the deposition rate of 100 ps in this simulations refers to a deposition rate of 800 ps (8 corner facets×100 ps) at most on one facet. At this slower deposition rate on a single facet, relative to the average time for the deposited atoms to diffuse to the other facets, a considerable number of adatoms is likely to diffuse from the borders of the corner facets to the edges and other facets of the cubical system. (c) A truncated cube is obtained when adatoms are deposited with a rate of one atom each 150 ps, corresponding to a maximum probable deposition rate of 1200 ps on a single facet. At this deposition rate, each single atom on {111} facet has time to diffuse and then occupy all adsorption sites on {110} facets, and then a new layer on {111} facet starts to grow. Here we have to remind that formation of a truncated cube requires further fine tuning of the relative diffusion and deposition rates as the process also involves diffusion of the adatoms along the <110> channels. The average diffusion time for an adatom in this channel is found to be approximately 1300 ps. (d) When the deposition rate is almost two times the inter-facet diffusion time ($\approx$ 500 ps), a transition from a cubic to a cuboctahedron structure is observed because at this relatively slow deposition rate the adatoms can easily diffuse from the corner sites to the cubic edges and side facets long before initiating small clusters on the {111} facets.

We have conducted similar growth simulations on Type II cubic system and found also that the growth of the seed is primarily dictated by the characteristics of the mobility of the adatoms on the seed facets (see Fig. S4). As discussed in the previous section, the factor that determines the growth path is the average time for an adatom to diffuse to the neighboring facets once deposited on the corner of the cube. When compared to the case on Type I system the pronounced effect of local morphology of the facet on the average diffusion time is clearly seen (see Table 3 and 4): the extra <110> channel on the edges of the Type II cubic system reduces the time by about nine-fold at 300 K, five-fold at 400 K, and three-fold at 500 K. Since at 500 K it takes for the adatom about 80 ps to cross the {111}/{110} edge, the deposition rate of one atom each 10 ps (8 corner facets × 10 ps = 80 ps) is calculated to be just enough to obtain an octopod shaped structure. Our

MD simulations with this specific deposition rate lead to a perfect octopod shaped cubic structure (Fig. S4). Our simulations also showed that corner facets of Type II cubic system first transform to Type I cubic system and then develop growth modes of Type I system with increasing deposition rate.

V. CONCLUSIONS

Regardless of the growth mode and the deposition rate, only a limited number of kinetic mechanisms form the atomistic basis of the earliest stages of growing nano-particles. Here, we have identified and illustrated such mechanisms to manipulate the growth kinetics in order to select a desired growth mode. This work not only reveals the underlying atomistic mechanisms behind the growth of specific metal nano-crystals but also provides new insight into their surface structure at the atomic scale. Based on the molecular static and dynamic calculations, it is apparent that the desired shape transformation of a metal nano-cube can be achieved once the surface mobility of a single atom on the corner facet is known. It is further found that trend in inter-facet mass transport depends on the characteristics of local morphology of the facets and does not change with increasing size of the nano-cube. In the particular cases of Type I and Type II cubic systems, the exchange of the adatom with an edge atom is found to be by far the determining atomistic mechanism in controlling the growth of the seeds.

However, one must keep in mind that the results presented here are for plain systems. Existence of defects and impurities in the seeds may change the growth paths and the energetics. There are also inherent factors involved in a synthesis process that effect the final shape of the end product: precursor, solvent, reducing agent, ligand agent, and capping agent. Change in concentrations of these ingredients alters the shape of final product[18, 19, 34]. Thus, a coordinated control of these factors is needed to engineer formation of nano clusters with specific shape. Since our goal in this work was to determine the single-atom processes that are crucial in defining the growth paths of nanoclusters, we have focused on the bare systems. However, further calculations involving various agents will help us put our understanding of the atomic nature of the observed growth modes on a firmer footing.

ACKNOWLEDGMENTS

This work was supported by the Scientific and Technological Research Council of Turkey-TUBITAK under Grant No. 109T105. Computations were carried out through the National Center for High Performance Computing, located at Istanbul Technical University, under Grant No. 20132007.

---

[1] S. Nie and S.R. Emory, *Science*, 1997, **275**, 1102.

[2] L.N. Lewis, *Chem. Rev.*, 1993, **93**, 2693.

[3] S. Leenders, R. Gramage-Doria, B. Bruin and J. Reek, *J. Chem. Soc. Rev.*, 2015, **44**, 433.

[4] Y. Nishihata, J. Mizuki, T. Akao, H. Tanaka, M. Uenishi, M. Kimura, T. Okamoto and N. Hamada, *Nature*, 2002, **418**, 164.

[5] R. Narayanan and M. El-Sayed, *Nano Lett.*, 2004, **4**, 1343.

[6] M.A. Reed, C. Zhou, C.J. Muller, T.P. Burgin and J.M. Tour, *Science*, 1997, **278**, 252.

[7] Y. Xia, X. Xia and H-C. Peng, *J. Am. Chem. Soc.*, 2015, **137**, 7947.

[8] A.R. Tao, S. Habas and P. Yang, *Small*, 2008, **4**, 310.

[9] B. Lim and Y. Xia, *Angew. Chem. Int. Ed.*, 2011, **50**, 76.

[10] H-C. Peng, S. Xie, J. Park, X. Xia X. and Y. Xia, *J. Am. Chem. Soc.*, 2013, **135**, 3780.

[11] Y. Sun and Y. Xia, *Science*, 2002, **298**, 2176.

[12] S. Xie, X.Y. Liu and Y. Xia, *Nano Research*, 2015, **8** 82.

[13] T. Sau and F.A. Rogach, *Adv. Mater*, 2010, **22**, 1781.

[14] M-R. Gao, Y-F. Xu, J. Jiang and S-H. Yu, *Chem. Soc. Rev.* , 2013, **42**, 2986.

[15] Z. Zhang, Z.Wang, H. Zhang, C. Wang, Y. Yin and M. Jin, *Nanoscale*, 2014, **6**, 3518.

[16] F. Baletto, C. Mottet and R. Ferrando, *Surface Science*, 1999, **446** 31.

[17] S.Valkealahti and M. Manninen, *Phys. Rev. B*, 1998, **57**, 15533.

[18] S. Xie, H. Zhang, N. Lu, M. Jin, J. Wang, M.J. Kim, Z. Xie, and Y. Xia, *Nano Lett.*, 2013, **13**, 6262.

[19] Y. Wang, S. Xie, J. Liu, J. Park, C. Z. Huang, and Y. Xia, *Nano Lett.*, 2013, **13**, 2276.

[20] X. Xia, S. Xie, M. Liu, H-C. Peng, N. Lu, J. Wang, M.J. Kim and Y. Xia, *Proc. Natl. Acad. Sci.*, 2013, **110**, 6669.

[21] Y. Xia, Y. Xiong, B. Lim and S. Skrabalak, *Angew. Chem. Int. Ed.*, 2008, **48**, 60.

[22] S.M. Foiles, M.I. Baskes and M.S. Daw, *Phys. Rev. B*, 1986, **33**, 7983; M.S. Daw, S.M. Foiles and M.I. Baskes, *Mater. Sci. Rep.*, 1993 **9**, 251.

[23] D. Wang, J. Zhao, S. Hu, X. Yin, S. Liang, and S. Deng, *Nano Lett.*, 2007, **7**, 1208; W. Liang, M. Zhou, *Phys. Rev. B*, 2006, **73**, 115409.

[24] B. Onat, M. Konuk, S. Durukanoglu and G. Dereli, *Nanotechnology*, 2009, **20**, 075707.

[25] M. Konuk and S. Durukanoglu, *Nanotechnology*, 2012, **23**, 245707.

[26] N-F. Yu, N. Tian, Z-Y. Zhou, L. Huang, J. Xiao, Y-H. Wen and S-G. Sun, *Angew. Chem. Int. Ed.*, 2014, **53**, 5097.

[27] J. Yang, W. Hu, S. Chen and J. Tang, *J. Phys. Chem. C*, 2009, **113**, 21501.

[28] Z.S. Pereira and E.Z. da Silva, *J. Phys. Chem. C*, 2011, **115**, 22870.

[29] W.G. Hoover, *Phys. Rev. A*, 1985, **31**, 1695.

[30] S. Nosé, *J. Chem. Phys.*, 1984, **81**, 511.

[31] S. Plimpton, *J. Comp. Phys.*, 1995, **117**, 1.

[32] G. Mills and H. Jónsson, *Phys. Rev. Lett.*, 1994, **72**, 1124.

[33] G. Mills, H. Jónsson and G.K. Schater, *Surf. Sci.*, 1995, **324**, 305.

[34] C. R. Bealing, W. J. Baumgardner, J.J. Choi, T. Hanrath, and R. G. Hennig, *ACS Nano*, 2012, **6**, 2118.

FIGURES

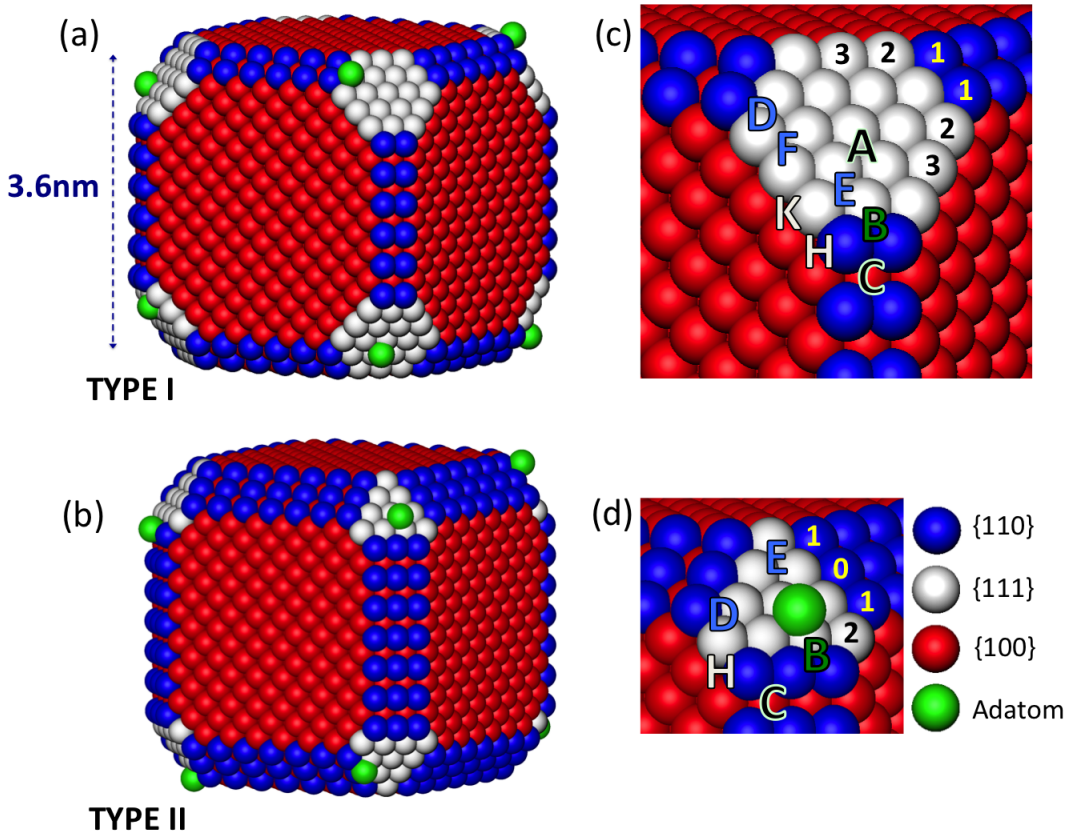

Fig. 1. The geometries of simulated cubic Ag nano-particles. While Type I cubic cell contains two chains of atoms along the <110> edges of the cube (a), Type II possesses three chains of atoms (b). The adsorption sites and labeling of the edge atoms on the {111} corners of Type I (c) and of Type II cubic system (d). The length of a side for both computational cells is taken to be 3.6 nm.

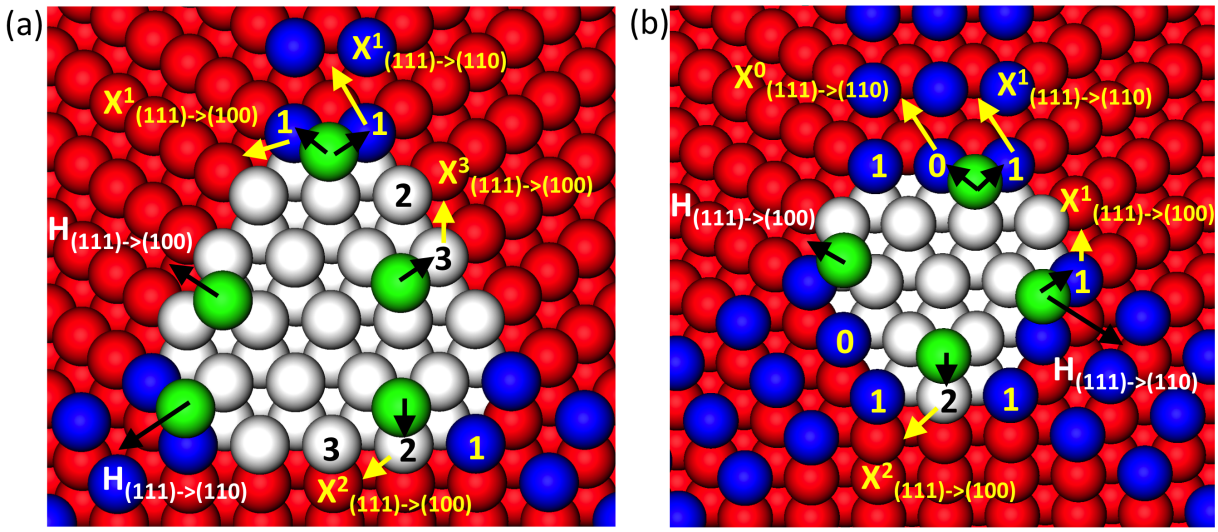

Fig. 2. The investigated diffusion processes on (a) Type I and (b) Type II systems. Green spheres represent mobile atoms and arrows indicate reaction directions of the regarding process. Gray and blue spheres denote the {111} and {110} facet atoms, respectively. Here H stands for the hopping whereas X shows the exchange process. Superscripts in exchange mechanisms demonstrate the edge atoms involved in the respective diffusion event. Subscripts, on the other hand, indicate border-crossing path from/to facets.

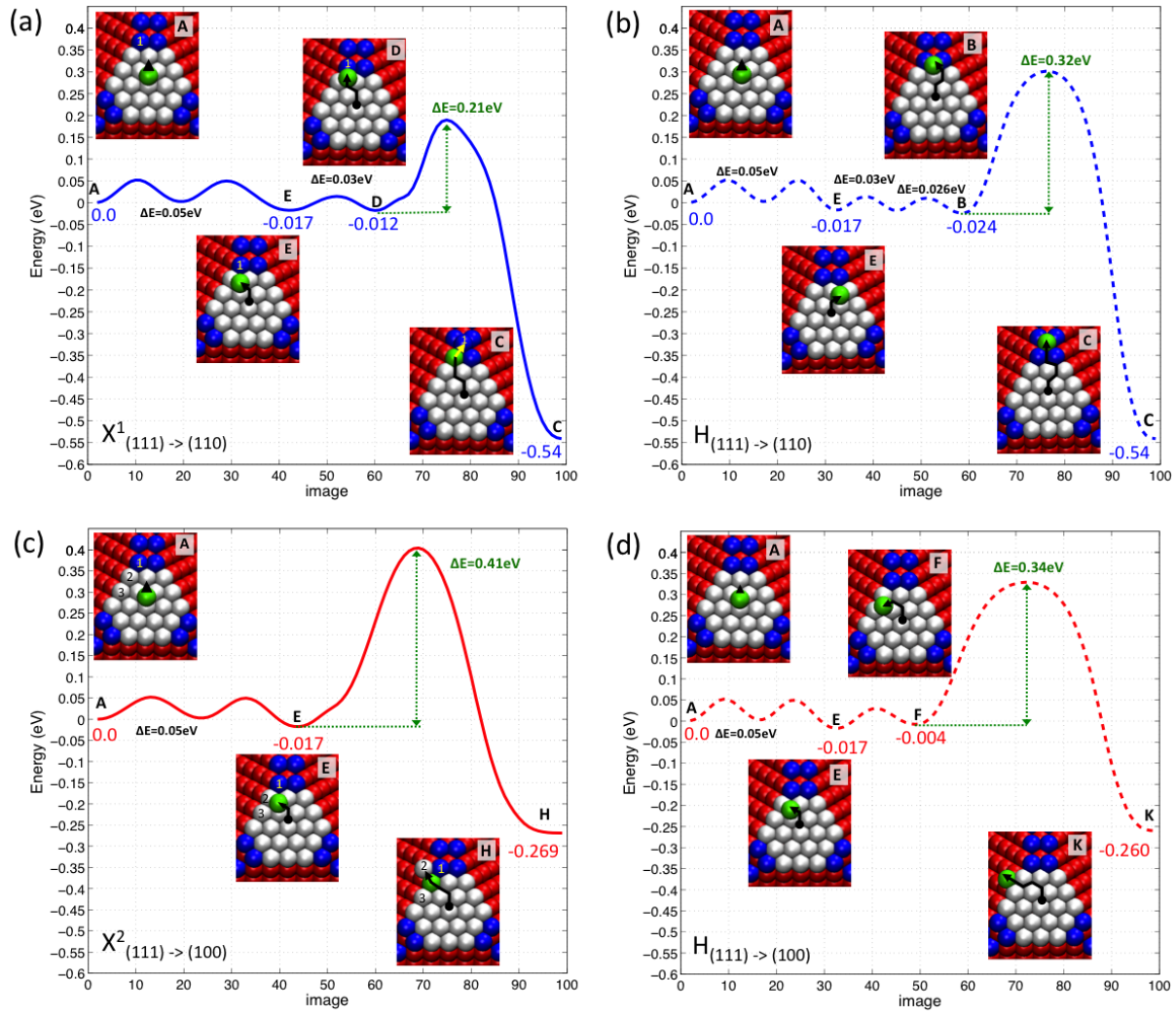

Fig. 3. The potential energy profile of an adatom along the diffusion path from the center of {111} to a nearby adsorption sites on the neighboring facets: (a) exchange to {110} via atom 1 or (b) hopping to {110} and (c) exchange to {100} via atom 2 or (d) hopping to {100} (see also Fig. 1 and Table 1). Energy zero is the energy of the system when the adatom (green sphere) is absorbed on the site A and the relative energies of other sites are given with respect to A. The inset figures show the snapshots of the system in the process.

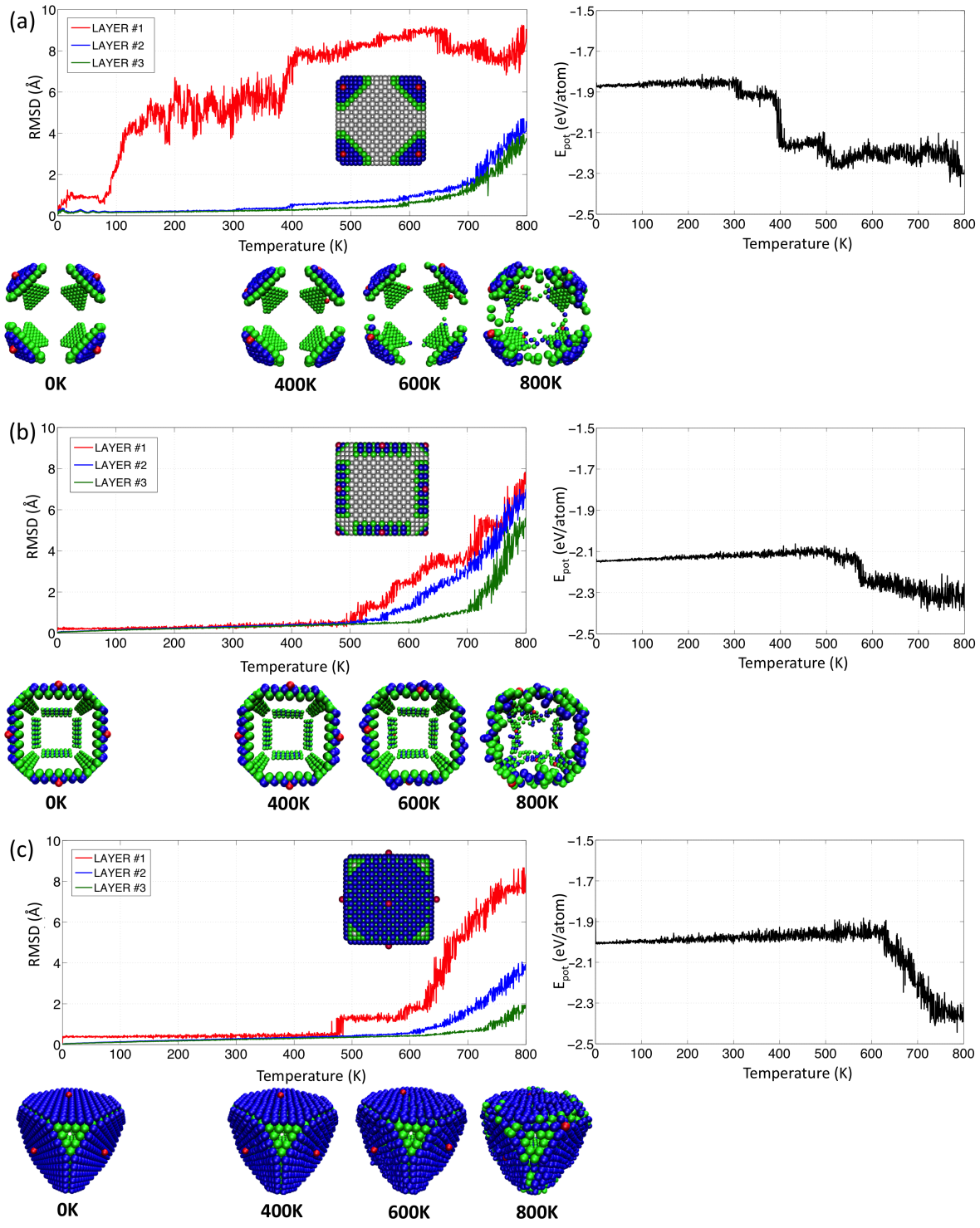

Fig. 4. The root mean square displacements (RMSD) of the first (adatoms), second, and third layer atoms of each facet on Type I cubic system: (a) for eight {111} facets, (b) for twelve {110} facets, and (c) for six {100} facets. On the right, the average potential energy of adatom is given as a function of temperature.

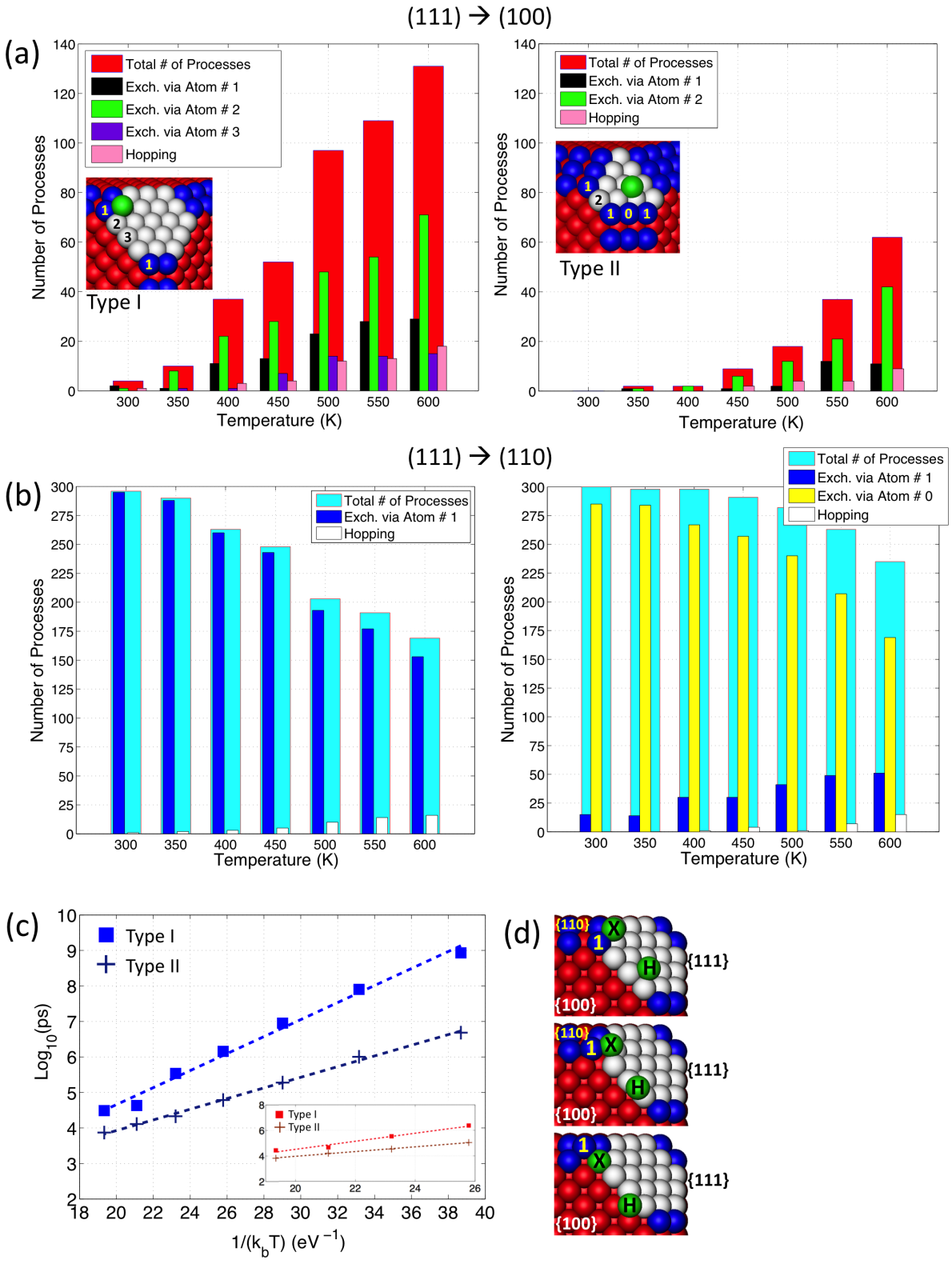
(111) → (100)
(a)
Total # of Processes
Exch. via Atom # 1
Exch. via Atom # 2
Exch. via Atom # 3
Hopping
Type I
Type II
Number of Processes
Temperature (K)
(111) → (110)
(b)
Total # of Processes
Exch. via Atom # 1
Exch. via Atom # 0
Hopping
(c)
Type I
Type II
Log10(ps)
1/(kbT) (eV−1)
(d)
{110}
{111}
{100}
X
H

Fig. 5. Statistical characteristics of 300 repeated single-atom diffusion events at varying temperatures: (a) Number of diffusion events from {111} to {100} facets (Type I on the left and Type II on the right). The inset shows the corner views of the Ag nano-cubes. (b) Number of diffusion events from {111} to {110} facets (similarly, Type I on the left, Type II on the right). (c) Arrhenius plots of the transition time for adatom-diffusion events to {110} and {100} facets. Blue marks stand for the transitions from {111} to {110} facets whereas red marks represent transitions from {111} to {100} facets. Dashed lines are the fitted values. (d) Possible diffusion mechanisms for an adatom diffusion from the {111} facet to the neighboring facets. In a hopping mechanism (H), the adatom simply jumps from a lattice site on the {111} facet to the closest one on the neighboring {100} and {110} facets, while in an exchange mechanism (X), the adatom kicks the atom below to the next site on the nearby facet and takes its place.

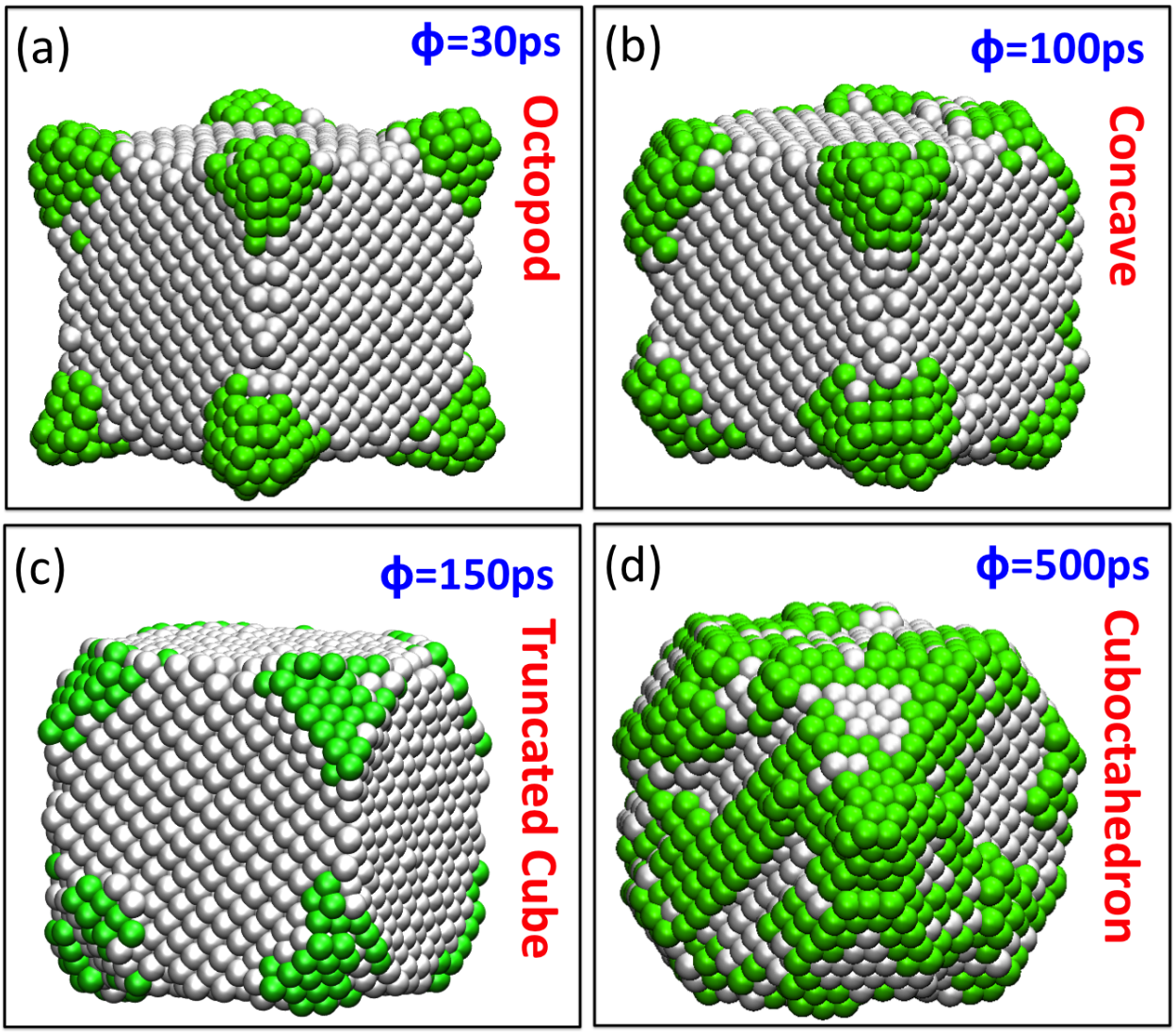

Fig. 6. Four specific growth modes of Ag nanocluster obtained at T=500 K: (a) an octopod after the deposition of 500 atoms with a deposition rate of one atom each 30 ps, (b) a concave after the deposition of 500 atoms with a deposition rate of one atom each 100 ps, (c) a truncated cube after the deposition of 200 atoms with a deposition rate of one atom each 150 ps, (d) a cuboctahedron after the deposition of 700 atoms with a deposition rate of one atom each 500 ps. Here Φ shows deposition rates at each specific growth simulation. The lighter atoms belong to initial configuration of cubic Ag cluster while the deposited atoms are shown by green color.

TABLES

Table 1. Adsorption energies, relative to the energy for the center site A, of various sites on the facets of cubic Ag clusters. For the selected adsorption sites (indicated in parentheses) see Fig. 1.

Adsorption site	Type I	Type II
Center on {111} facet, *fcc* (A)	0.000	0.000
{110} / {100} submit on {111} facet, *hcp* (D)	-0.012	-0.016
Edge on {111} facet, *fcc* (E)	-0.017	-0.021
Edge on {111} facet, *hcp* (F)	-0.004	——
Corner on {111} facet, *fcc* (B)	-0.024	-0.018
Corner on {110} facet, (C)	-0.541	-0.526
Edge on {100} facet close to {110} / {100}, (H)	-0.269	-0.270
Edge on {100} facet, (K)	-0.260	——

Table 2. Calculated activation barriers (in eV) for several single atom diffusion mechanisms on the surfaces of Ag Type I and Type II cubic systems. Here X and H stand for exchange and hopping mechanism, respectively. The superscripts represent the participating substrate atoms in the exchange processes.

Mechanism	Type I	Type II
$X^0_{(111)\rightarrow(110)}$	-	0.15
$X^1_{(111)\rightarrow(110)}$	0.21	0.23
$H_{(111)\rightarrow(110)}$	0.32	0.34
$X^1_{(111)\rightarrow(100)}$	0.39	0.39
$X^2_{(111)\rightarrow(100)}$	0.41	0.41
$X^3_{(111)\rightarrow(100)}$	0.43	-
$H_{(111)\rightarrow(100)}$	0.34	0.33

Table 3. For Type I system, number of diffusion events and regarding average diffusion times as a function of temperature.

Temperature	300 K	350 K	400 K	450 K	500 K	550 K	600 K
From (111) to (110)							
Average Time	7577 ps	2708 ps	1045 ps	472 ps	254 ps	103 ps	79 ps
Total # of Atom	296	290	263	248	203	191	169
From (111) to (100)							
Average Time	10108 ps	3305 ps	1221 ps	589 ps	252 ps	106 ps	85 ps
Total # of Atom	4	10	37	52	97	109	131

Table 4. For Type II system, number of diffusion events and regarding average diffusion times as a function of temperature.

Temperature	300 K	350 K	400 K	450 K	500 K	550 K	600 K
From (111) to (110)							
Average Time	800 ps	405 ps	196 ps	120 ps	76 ps	61 ps	46 ps
Total # of Atom	300	298	298	291	282	263	235
From (111) to (100)							
Average Time	-	-	-	155 ps	93 ps	67 ps	46 ps
Total # of Atom	0	2	2	9	18	37	65